STM JOURNALS

Journal of
Materials & Metallurgical Engineering

ISSN: 2231-3818 (Online)
ISSN: 2321-4236 (Print)
Volume 12, Issue 1, 2022
DOI (Journal): 10.37591/JoMME

http://engineeringjournals.stmjournals.in/index.php/JoMME/index

Research JoMME

Advanced Quantitative Analysis of Dynamic Recovery during Warm Working of FCC Alloys

Prantik Mukhopadhyay*

Abstract

Metal working processes of warm working require an advanced quantitative analysis of dynamic and static recovery of dislocations to control microstructures and crucial shape forming properties. Feasibility of dynamic recovery by thermal glide and static recovery by climb of constricted jogs, applicable to ausforming, nano bulk forming by SPD and normalizing has been addressed to design new steels, used for hulls, and tribologically superior bearings. Predictive dislocation recovery analysis shows Taylor factor as an important dynamic recovery controller for mean dislocation dynamics and crystallographic orientation dependent dislocation dynamics to govern work hardening and recovery strain rate of materials. Taylor factor has been defined as glide plane specific stacking fault energy. In contrast to static recovery by climb, present mechanism has found that less stacking fault energy will have enhanced dynamic recovery kinetics. Predicted recovery kinetics has been qualitatively validated by frequency of low angle boundaries, formed during ausforming and normalizing, in regard to Taylor factors of crystallographic orientations of retained austenite, detected by EBSD.

Keywords: Aluminium alloys, ausforming, Bainitic steel, dislocation dynamics and recovery, FCC alloys, SPD

INTRODUCTION

Use of predictive dislocation recovery has been gradually become crucial to industrialize new metal working processes [1]. Microstructural mechanisms concordant to dynamic recovery has been defined recently [2, 3]. Kubin and his co-workers have tried to emphasize the effect of strain rate, temperature, and crystallographic orientation dependent annihilation distance of screw dislocations in dynamic recovery. Bacroix and her co-workers introduced the crystallographic orientation dependent dynamic recovery of dislocations using Kocks-Mecking theory.

Benefit of dynamic recovery is generally drawn in metal working to increase workability. Warm working is liable to incorporate non-compact slip in FCC while only compact slip is relented. Non-compact slip on {110} and {100} crystallographic planes as well as the compact slip on {111} crystallographic planes is in favor of greater dynamic recovery kinetics and workability [4, 5]. Ausforming of bainitic steel is liable to be known as an industrial warm metal working practice where FCC austenite phase is worked at 573–623 K and decomposed to bainite by mechanical driving force from dislocations [6]. Rapid dynamic recovery of dislocations is attributed to the mechanism of the rate controlling conservative kink movements by thermal glide [7]. High stress applied to form nano bulk by SPD is used to commensurate an increased working temperature.

*__Author for Correspondence__
Prantik Mukhopadhyay

Scientist, Electron Microscopy Group, Defence Metallurgical Research Laboratory, Kanchanbagh, Hyderabad, Telangana, India

Received Date: January 28, 2022
Accepted Date: March 05, 2022
Published Date: March 15, 2022

Citation: Prantik Mukhopadhyay. Advanced Quantitative Analysis of Dynamic Recovery during Warm Working of FCC Alloys. Journal of Materials and Metallurgical Engineering. 2022; 12(1): 1–14p.

Industrial multi-step warm working practices are used to incorporate intermittent continuous cooling when dislocations are recovered statically by non-conservative movements or climb of constricted jogs. Metal working practices in industry inevitably require an eminent and robust physical based simulator to address dynamic and static recovery. An advanced quantified mechanism of dynamic and static recovery to predict dislocation density during the multi-step warm working of FCC alloys to fabricate nano bainite and nano bulk by SPD is envisaged and validated. Dynamic recovery by mean dislocation kinetics and crystallographic orientation dependent dislocation dynamics of FCC alloys is required to be mitigated in simulation for fabrication of hulls and tribologically superior bearings.

MATERIALS AND METHODS

High hardness bainitic steel with composition shown in Table 1, was melted, cast in foundry, rolled at about 1100 K–900 K and normalized in air.

Table 1. Composition in weight percent.

C	Mn	Si	Ni	Cr	Mo
0.70	2	2	2	2	0.50

Electron Backscatter Diffraction (EBSD) study was performed using Carl Zeiss make SUPRA 55, Scanning Electron Microscope with Field Emission Gun to measure pre-dominant FCC austenite, BCT and BCC phases.

Normal sample preparation methods of grinding by emery papers and polishing by colloidal silica solution were performed. Polished samples with sample reference Normal Direction, ND, and Rolling Direction, RD were used for EBSD study with step size 0.15 µm. Special BCT phase parameter file, shown in Table 2, was employed for detecting BCT and BCC phases simultaneously, since the use of BCC phase parameter files used to generate higher mean angular deviations in Kikuchi patterns than BCT phase parameter files, confirmed by extensive trial experiments for known martensitic structure. Pre-dominant FCC, BCT, and BCC phases are shown in Figure 1.

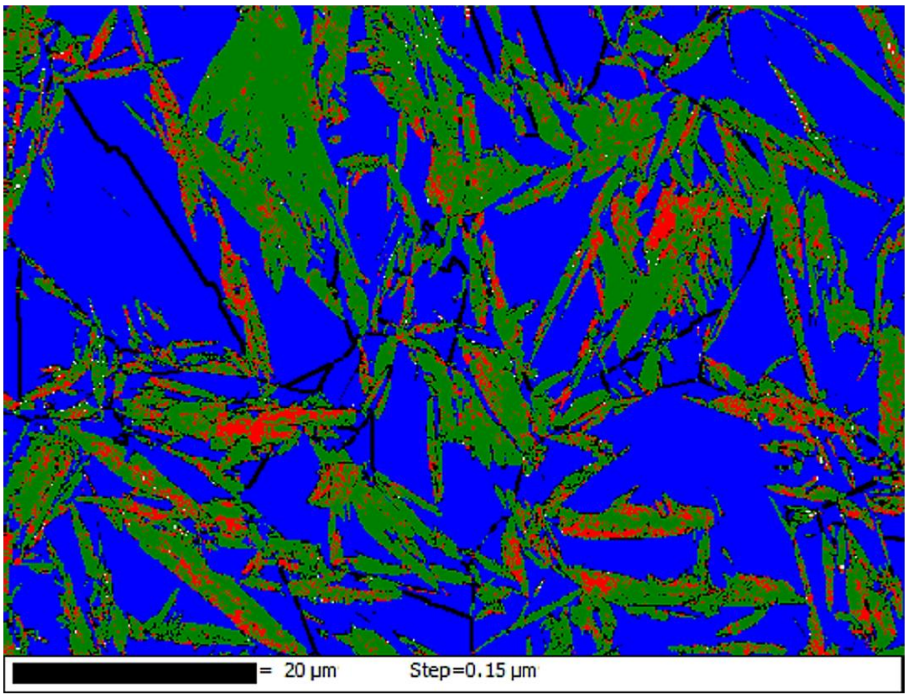

Figure 1. Pre-dominant matrix phases of ausformed bainite, FCC retained Austenite: Indigo Blue, BCT: Green and BCC: Red, high angle boundaries: Black.

Table 2. The BCT phase parameter file.

L_1	L_2	L_3	Atom positions	Space group
0.2857 nm	0.2857 nm	0.2948 nm	(000), $\left(\frac{1}{2}\frac{1}{2}\frac{1}{2}\right)$	I4 mmm (I 139)

Representative crystallographic texture of majority of retained austenite grains, analysed and represented in Euler space by an equal ϕ_2 sections of 0°, 45°, and 65° in Figure 2, found to be with an angular scatter of ~20º from $\{011\}||ND$and $\{111\}||ND$ fibres.

Frequency of low angle boundaries, Taylor factor, T_f, distribution were analysed by EBSD-HKL software in regard to FCC retained austenite, delineated in Figure 3. Grains with the highest T_f are dynamically recovered to an extent greater than grains with the lowest T_f.

AUSFORMED BAINITIC STEEL: RECOVERY KINETICS TREND FROM EXPERIMENT

Ausformed bainitic steel was normalized in air. During continuous cooling to room temperature, austenite was decomposed to BCC and low temperature BCT phases.

Pre-dominant matrix phases (Figure 1), FCC retained austenite, BCC ferrite, and BCT phase were characterized by EBSD technique. Crystallographic texture of retained austenite phase has been found near α-fibre, $\{011\}||ND$fibre and γ-fibre, $\{111\}||ND$ fibre with an angular scatter ~20°, addressed in Figure 2.

Dislocations recovered dynamically during ausforming and statically during normalizing in air. Frequency of low angle boundaries and Taylor factor map of retained austenite showed with fidelity that low angle boundaries >0.5° are higher in crystallographic orientations with lower T_f factors, compared to that of crystallographic orientations with higher T_f factors, in dynamically and statically recovered specimen (Figure 3). Greater percentage of BCC and BCT phases in crystallographic orientations with lower T_f factors confirms that the mechanical driving force from dislocations after recovery enhanced the decomposition process of FCC austenite phase. Dislocations in form of low angle boundaries, distributed in larger scale, rather than their presence merely near decomposed inter-faces, are liable to prove that they are not just misfit dislocations.

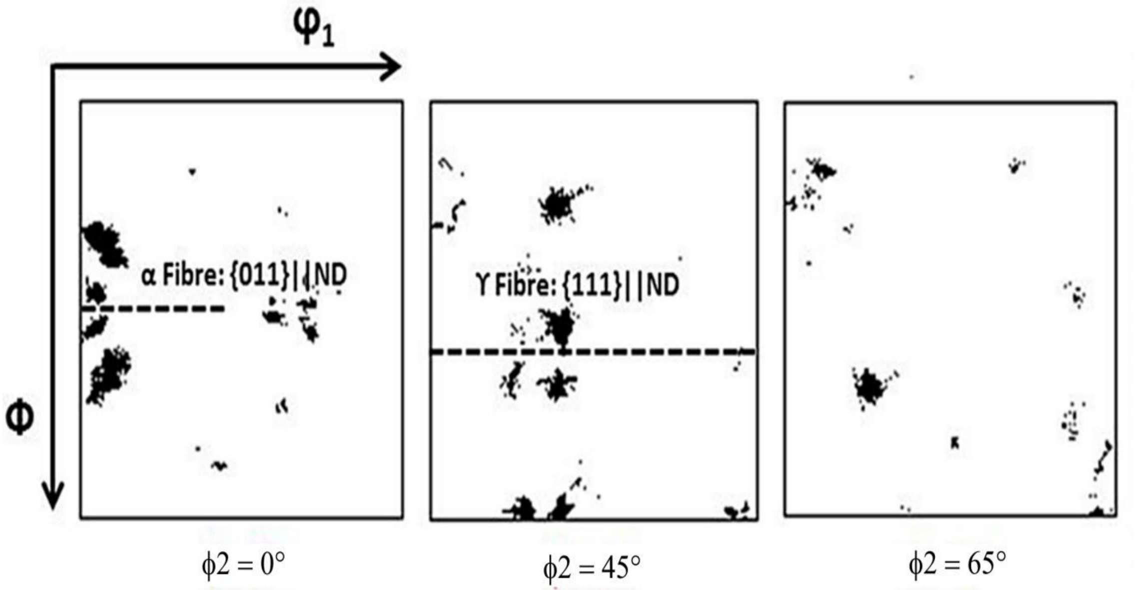

Figure 2. Crystallographic texture of retained austenite in Euler space by an equal ϕ_2 sections of 0°, 45°, and 65°.

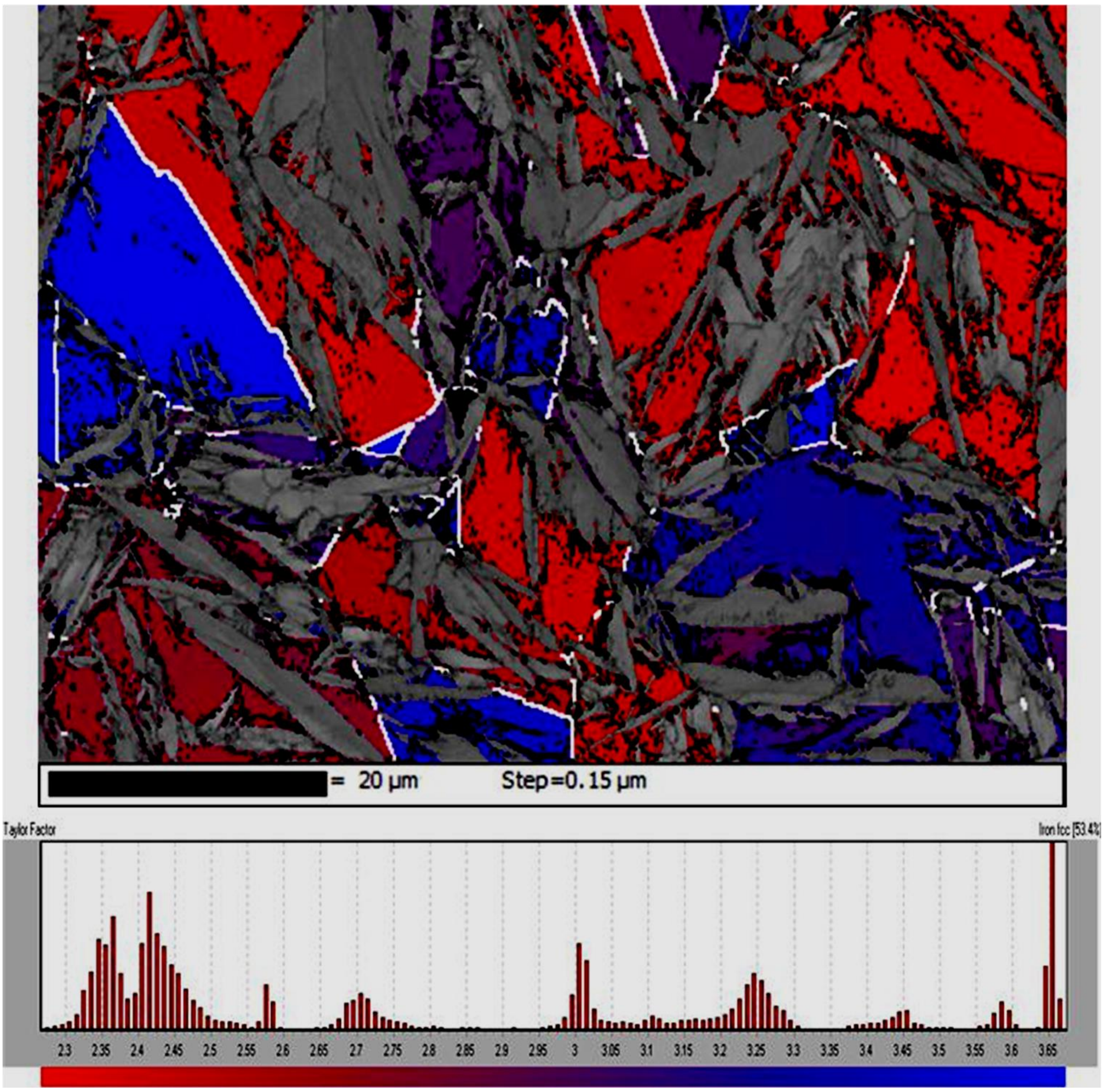

Figure 3. Taylor factor distribution, dynamically less recovered Black Orange: lowest Taylor factor 2.27 and recovered Indigo Blue: highest Taylor factor 3.67 of retained austenite with low angle > 0.5° boundaries in black and high angle >15° boundaries in white.

ADVANCED QUANTITATIVE ANALYSIS

Dynamic Recovery Kinetics

Kinks are jogs on glide planes. Jogs with lengths equal to one burger vector, b are known as unit jogs. Kinks with lengths greater than unit jogs are known as superjogs. Jogs of radius R are liable to glide conservatively on slip planes [7]. Industrial hot and warm working is often known to meet rapid dynamic recovery, governed by mechanical energy and thermal energy.

Figure 4(a)–(b) is an intrinsic dynamic recovery regiment of kinks on glide planes where kinks obtain an essentially stable state from their inter-mediate unstable state, specified by an energy gradient, to traverse an infinitesimal distance. Dislocation gliding velocity, during dynamic recovery from planar energy gradient has been estimated by an advanced Hirth and Lothe mechanism [7].

$$\upsilon \approx \frac{2D}{\rho_0 f} e^{\left(\frac{\sigma b f l}{T_f k T}\right)} \tag{1}$$

Journal of Materials & Metallurgical Engineering
Volume 12, Issue 1
ISSN: 2231-3818 (Online), ISSN: 2321-4236 (Print)

where, the rare event probability of finding mutually opposite dislocations in an intrinsic concerned area per unit area of the bulk is $\frac{1}{0.5\rho_0}$, when the initial dislocation density is ρ_0, D is diffusivity, b is burger vector, T_f is Taylor factor, $f \approx S_D$ is the traversed distance $f = \lambda b$, when λ is a constant, σ is normal stress, l_J is the distance between pinning jogs, k is Boltzmann constant, S_D is the dislocation spacings, and T is the temperature.

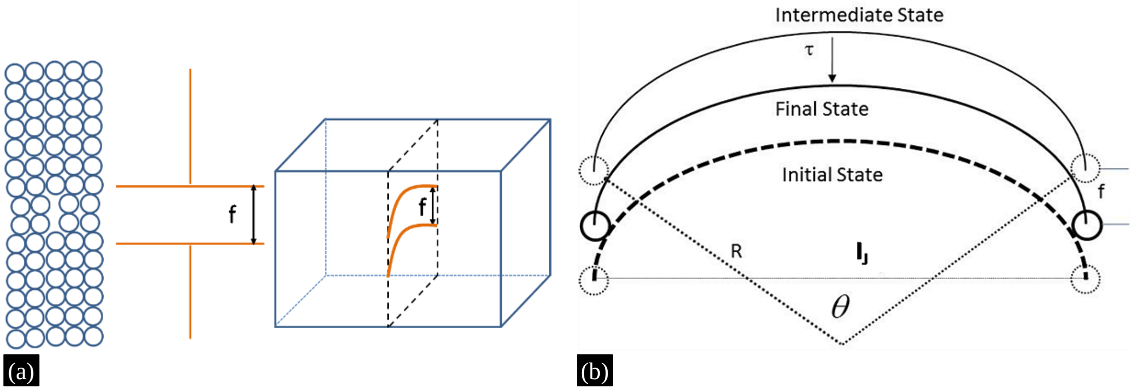

Figure 4. Glide of kinks. (a) Representative lattice with kinks on glide plane of spacing f. (b) l_J is the distance between pinning jogs, q is the angle in radian, dislocation regiment radius R, and planar stress gradient, τ, constricted by stacking fault energy, γ_{SFE}.

An intrinsic interactive concerned volume specified by bl_Jf, where the distance between two pinning jogs is

$$l_J = \eta b = \frac{R}{\mu(\tau)} \tag{2}$$

where η an extended jog constant, R is the radius of dislocation regiment, and $\mu(\tau)$ is an intrinsic stress dependent constant.

Radius of dislocation regiment is

$$R = \frac{l_R}{\theta} = \frac{\kappa}{\theta\rho^{\frac{1}{2}}} \tag{3}$$

where l_R is the curved length of the dislocation regiment $\kappa$is an extensive Frank loop constant, and ρ is dislocation density. Angle θ radian driven sinusoidal ratio derivative

$$sin(28.66\theta) = \frac{l_R}{2R} = \frac{1}{2\mu(\tau)} \tag{4}$$

The intrinsic constant

$$\mu(\tau) = \frac{1}{2\,sin(28.66\theta)} \tag{5}$$

The normal stress

$$\sigma = \alpha G b \rho^{\frac{1}{2}} \tag{6}$$

where G is shear constant and α is 0.5 [1].

Therefore, the velocity of the dislocation during recovery is

$$\upsilon = \frac{2D}{\lambda b \rho_0} exp\left(\frac{\eta\lambda b^3\sigma}{T_f kT}\right) = \frac{2D}{\lambda b \rho_0} exp\left(\frac{\eta\lambda b^3\alpha G b\rho^{\frac{1}{2}}}{T_f kT}\right) \tag{7}$$

From Eqn. 6

$$\rho = \left(\frac{\sigma}{\alpha G b}\right)^2 \tag{8}$$

The dynamic recovery kinetics is at an applied strain rate $\dot{\varepsilon}$

$$-\frac{d\rho}{dt} = -\frac{d}{dt}\left(\frac{\sigma}{\alpha G b}\right)^2 = -\frac{2\sigma}{(\alpha G b)^2}\frac{d\sigma}{dt} = -\frac{2}{(\alpha G b)^2}\frac{\sigma}{\tau}\frac{\tau}{b}b\frac{d\sigma}{d\varepsilon}\frac{d\varepsilon}{dt} = -\frac{2b\mu(\tau)G}{(\alpha G b)^2}{T_f}^3\frac{G}{R}\dot{\varepsilon} \tag{9}$$

From Taylor theory [4]

$$\frac{\sigma}{\tau} = \frac{\gamma}{\varepsilon} = T_f \tag{10}$$

and

$$\frac{\tau}{b} = \frac{G}{l_J} \tag{11}$$

where τ is the shear stress and $\gamma$is the shear strain.
An estimated Taylor hardening

$$\frac{d\sigma}{d\varepsilon} = \frac{d\sigma}{d\tau}\frac{d\tau}{d\gamma}\frac{d\gamma}{d\varepsilon} = {T_f}^2 G \tag{12}$$

Strain rate is

$$\dot{\varepsilon} = -\frac{\dot{\gamma}}{T_f} = -\frac{b\rho\upsilon}{T_f} \tag{13}$$

where $\dot{\gamma}$ is the shear strain rate.

R is addressed as an intrinsic balance of dislocation line force per unit length, $T_l R$ and stacking fault energy per unit area, γ_{SFE} [8].

$$T_l = \frac{\gamma_{SFE}}{R} \tag{14}$$

Expressing dislocation line stress as normal stress

$$T_l = \alpha G b \rho^{\frac{1}{2}} = \frac{\gamma_{SFE}}{R} \tag{15}$$

Therefore,

$$\gamma_{SFE} = \alpha G b \rho^{\frac{1}{2}} R = \frac{\alpha G b^2}{R}\rho^{\frac{1}{2}}\frac{R^2}{b} = \frac{\alpha G b^2}{R} \tag{16}$$

where

$$\frac{R^2}{b}\rho^{\frac{1}{2}} = 1 \tag{17}$$

For unit jogs of Figure 4(a) with an atomic stacking fault spacing, $\rho = \frac{1}{b^2}$, adsorbed to the trend of radius of the unit jogs $R = b$. Taylor factor is expressed as stacking fault energy of curved dislocations.

$$T_f = \frac{\sigma}{\tau} = \frac{\alpha G b \rho^{\frac{1}{2}}}{\tau} = \alpha \rho^{\frac{1}{2}} l_B = \frac{\alpha \rho^{\frac{1}{2}} R}{\mu(\tau)} = \frac{\alpha \rho^{\frac{1}{2}} G b^2}{\gamma_{SFE}} = \frac{\alpha G b^2 \rho^{\frac{1}{2}}}{\gamma_{SFE}} = \frac{\sigma b}{\gamma_{SFE}} = \frac{T_f b \tau}{\gamma_{SFE}} \tag{18}$$

Since

$$T_f = \frac{\sigma b}{\gamma_{SFE}} = \frac{T_f b \tau}{\gamma_{SFE}} \tag{19}$$

$$\tau = \frac{\gamma_{SFE}}{b} \tag{20}$$

Therefore, for unit jogs of radius $R = b$

$$T_l = \sigma = \tau = \frac{\gamma_{SFE}}{R} = \frac{\gamma_{SFE}}{b} \tag{21}$$

Dynamic recovery kinetics updated as

$$-\frac{d\rho}{dt} = \frac{2b\mu(\tau)G}{(\alpha Gb)^2} T_f^3 \frac{\gamma_{SFE}}{\mu(\tau)b^2} \frac{b\rho\upsilon}{T_f} = \frac{2b\mu(\tau)G}{(\alpha Gb)^2} T_f^3 \frac{\gamma_{SFE}}{\mu(\tau)b^2} \frac{b\rho}{T_f} \frac{2D}{\lambda b\rho_0} exp\left(\frac{\eta\lambda b^3\alpha Gb\rho^{\frac{1}{2}}}{T_f kT}\right)$$

$$= \frac{4b^2G}{(\alpha Gb)^2} T_f^2 \frac{\gamma_{SFE}}{b^2} \rho \frac{D}{\lambda b\rho_0} exp\left(\frac{\eta\lambda b^3\alpha Gb\rho^{\frac{1}{2}}}{T_f kT}\right) = \frac{4DT_f{}^2\gamma_{SFE}\rho}{\lambda\alpha^2Gb^3\rho_0} exp\left(\frac{\eta\lambda b^3\alpha Gb\rho^{\frac{1}{2}}}{T_f kT}\right) \tag{22}$$

Therefore,

$$-\frac{d\rho}{dt} = \frac{4D\alpha^2G^2b^4\rho\gamma_{SFE}\rho}{\lambda\alpha^2Gb^3\gamma_{SFE}^2\rho_0} exp\left(\frac{\eta\lambda b^3\alpha Gb\rho^{\frac{1}{2}}}{T_f kT}\right) = \frac{4DGb\rho^2}{\lambda\gamma_{SFE}\rho_0} exp\left(\frac{\eta\lambda b^4\alpha G\rho^{\frac{1}{2}}\gamma_{SFE}}{\alpha Gb^2\rho^{\frac{1}{2}}kT}\right)$$

$$= \frac{4DGb\rho^2}{\lambda\gamma_{SFE}\rho_0} exp\left(\frac{\eta\lambda\gamma_{SFE}b^2}{kT}\right) = \frac{\rho^2}{\gamma_{SFE}} F(T) \tag{23}$$

Where,

$$F(T) = \frac{4DGb}{\lambda\rho_0} exp\left(\frac{\eta\lambda\gamma_{SFE}b^2}{kT}\right) \tag{24}$$

Therefore, dynamic recovery rate with time

$$\int_{\rho}^{\rho_t} \frac{d\rho}{\rho^2} = -\frac{F(T)}{\gamma_{SFE}} \int_0^t dt \tag{25}$$

$$-\frac{1}{\rho_t} + \frac{1}{\rho_0} = -\frac{F(T)}{\gamma_{SFE}} t$$

$$\frac{1}{\rho_t} = \frac{1}{\rho_0} + \frac{F(T)}{\gamma_{SFE}} t \tag{26}$$

Static Recovery Kinetics of Constricted Jogs

The velocity of jogs during non-conservative movement for being recovered due to mutually annihilated by jogs of opposite signs and to increase dislocation spacings S_D with time $t$by diffusive flux of atoms

$$\boldsymbol{\upsilon} = \frac{\boldsymbol{dS_D}}{\boldsymbol{dt}} = \boldsymbol{P_D} \frac{\boldsymbol{D}}{\boldsymbol{S_D}} = \boldsymbol{P_D} \frac{\boldsymbol{D_0\, exp\left(-\frac{Q_d}{kT}\right)}}{\boldsymbol{S_D}} \tag{27}$$

The rare event probability of occurrence of the concerned surface element per unit area of bulk is

$$P_D = \frac{1}{0.5\rho_0} \tag{28}$$

ρ_0 is the initial dislocation density

$$\upsilon = \frac{dS_D}{dt} = P_D \frac{D_0\, exp\left(-\frac{Q_d}{kT}\right)}{S_D} \tag{29}$$

The elastic energy of stacking fault, γ_{SFE} generally constricts jogs, diffusing atoms to cross the activation energy hill.

$$E_N = exp\left(\frac{Q_j\gamma_{SFE}}{kT}\right) \tag{30}$$

Active surface area of the elastic stress field of the stacking fault is

$$Q_j = \lambda_0 b^2 \tag{31}$$

where λ_0 is a constant.

Therefore, the effective non-conservative jog movement rate under the elastic stress field of the stacking fault

$$v = \frac{dS_D}{dt} = \frac{P_D D_0 \, exp\left(\frac{Q_j \gamma_{SFE} - Q_d}{kT}\right)}{S_D} \tag{32}$$

$$S_D dS_D = P_D D_0 \, exp\left(\frac{Q_j \gamma_{SFE} - Q_d}{kT}\right) dt \tag{33}$$

Hence, integrating the range of the dislocations spacing from S_{D0} to S_{Dt} for the time range from 0 to t

$$\int_{S_{D)}}^{S_{Dt}} S_D dS_D = P_D D_0 \, exp\left(\frac{Q_j \gamma_{SFE} - Q_d}{kT}\right) \int_0^t dt \tag{34}$$

$$\left[\frac{S_{Dt}^2 - S_{D0}^2}{2}\right] = P_D D_0 \, exp\left(\frac{Q_j \gamma_{SFE} - Q_d}{kT}\right) t \tag{36}$$

Since the dislocation density is denoted by the total length of dislocations per unit volume, therefore,

$$S_{D0}{}^2 = \frac{1}{\rho_0} \text{ and } S_{Dt}{}^2 = \frac{1}{\rho_t} \tag{37}$$

Therefore, the static recovery of the constricted jogs is expressed as

$$\frac{1}{\rho_t} - \frac{1}{\rho_0} = 2P_D D_0 \, exp\left(\frac{Q_j \gamma_{SFE} - Q_d}{kT}\right) t \tag{38}$$

$$\frac{1}{\rho_t} - \frac{1}{\rho_0} = 2P_D D_0 \, exp\left(\frac{\lambda b^2 \gamma_{SFE} - Q_d}{kT}\right) t \tag{39}$$

$$\frac{1}{\rho_t} = \frac{1}{\rho_0} + \frac{4}{\rho_0} D_0 \, exp\left(\frac{\lambda b^2 \gamma_{SFE} - Q_d}{kT}\right) t \tag{40}$$

Dynamic and Static Recovery Kinetics: Validity from Experiment

As postulated, the dynamic recovery kinetics of bainitic steel increases with thermal driving force of warm working, 900 K–1100 K, for the stacking fault energy range, 0.030–0.050 Jm^{-2}, put forth in Figure 5 (a)-(b). Dynamic recovery kinetics is liable to be rapid especially for less stacking fault energy and an expected greater thermal driving force of an industrial hot working. Fleeting warm working rolling procedure of reversing and tandem mills for few seconds from entry to exit is estimated to make precise dynamic recovery kinetics with predicted dislocation density difference of the order of 7.

Dynamic recovery rate of an industrially fabricated aluminum alloy, with stacking fault energy 0.130 Jm^{-2}–0.150 Jm^{-2}, is liable to pay an extremely unbreached rate of kinetics centre to predicted dislocation densities for routine warm and hot working at 423K–523K {Figure 5 (c)-(d)}. Classically stacking fault energy is defined by $\gamma_{SFE} = F_2Gb$, where F_2, G, and b are intensive material specific constants.

Industrial normalizing after warm rolling of bainitic steels from 900K to 300K, cooling at the rate of 50K per minute, is found to conserve dislocations liberally, without non-conservative austerity, delineated in Figure 5(e).

Journal of Materials & Metallurgical Engineering
Volume 12, Issue 1
ISSN: 2231-3818 (Online), ISSN: 2321-4236 (Print)

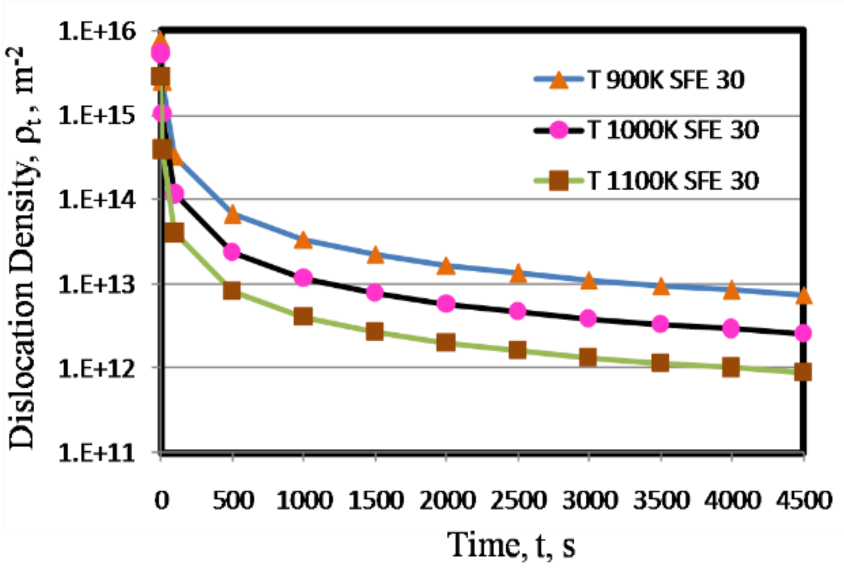

(a)

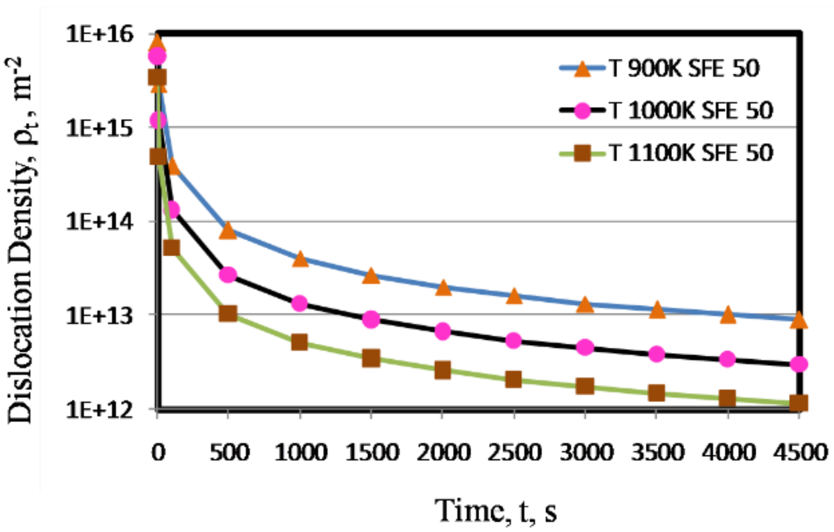

(b)

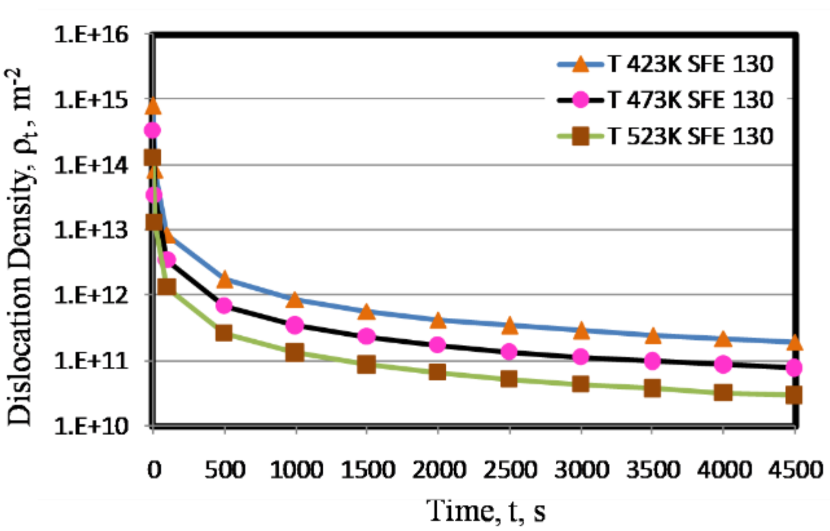

(c)

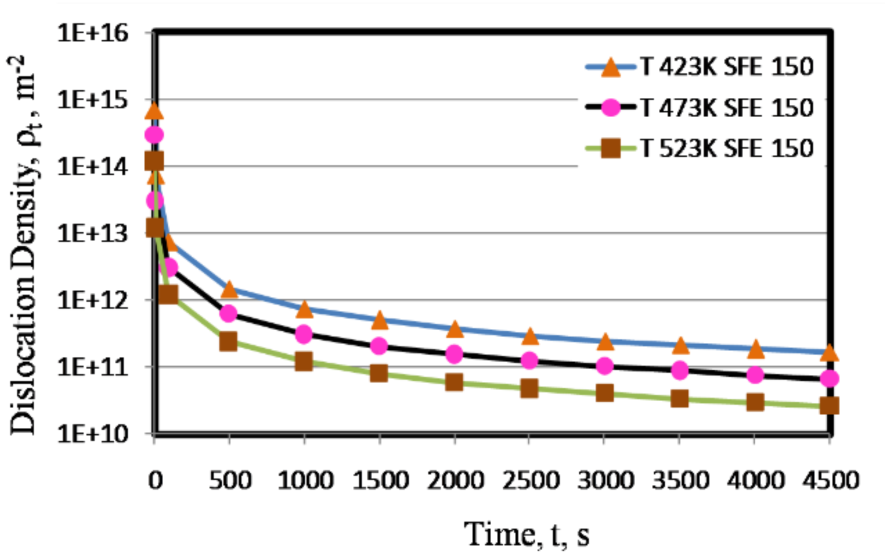

(d)

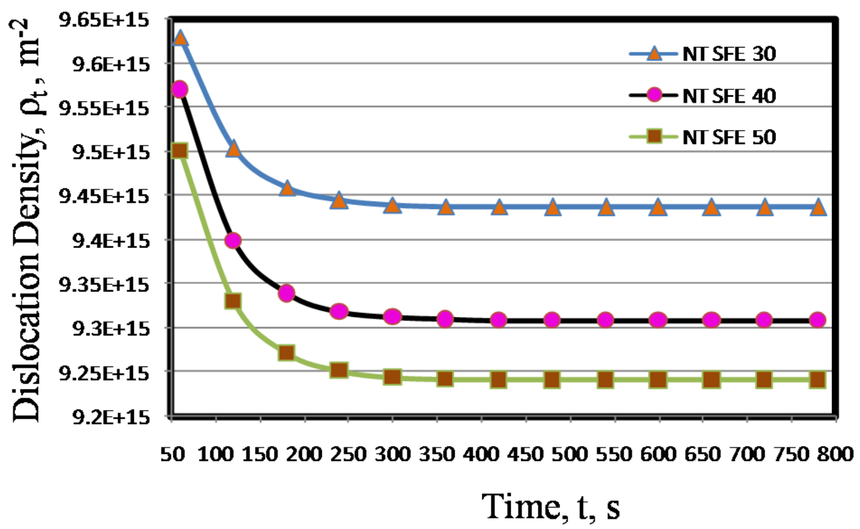

(e)

Figure 5. (a) Dynamic recovery of dislocations in steel stacking fault energy 0.030 Jm^{-2}, (b) Dynamic recovery of dislocations in steel stacking fault energy 0.050 Jm^{-2}, (c) Dynamic recovery of dislocations in aluminium alloy, stacking fault energy 0.130 Jm^{-2}, (d) Dynamic recovery of dislocations in aluminium alloy, stacking fault energy 0.150 Jm^{-2}. (e) Static recovery of dislocations in normalized steels, stacking fault energies 0.030 Jm^{-2}, 0.040 Jm^{-2} and 0.050 Jm^{-2}.

Present work defined T_f factor as inversely proportional to γ_{SFE} at a constant normal stress. Hence, the ascending order of planar γ_{SFE} is {111}-{011}-{001}. The ascending order of planar dynamic recovery rate is predicted by present analysis as {001}-{101}-{111}. The qualitative frequency of low angle boundaries obtained from dynamic and statically recovered sample shows that ascending trend of recovery rate is {001}-{101}-{111}, concordant to the quantified mechanism of present work. The static recovery kinetics by climb of extended jogs suggested that dislocation recovery is enhanced by higher γ_{SFE}, which is opposite to the effect of γ_{SFE} on dynamic recovery rate by thermal glide. Though the static recovery of crystallographic planes was enhanced by higher γ_{SFE} during normalizing in air, the dynamic recovery kinetics of less γ_{SFE} planes during ausforming was liable to be pre-dominant, so that the predicted trend of dynamic recovery is validated by dynamic recovery induced frequency of the low angle boundaries, even after normalizing.

DISCUSSION

Formulated dynamic recovery of dislocations during warm working is liable to resemble dynamic recovery by planar energy equilibrium. Crystallographic orientation dependent dynamic recovery [9–12] is governed by γ_{SFE}. Effect of γ_{SFE} in recovery is present in both pre-exponential and exponential terms. Effect of γ_{SFE} is found in pre-exponential term where low γ_{SFE} of {111} planes will reduce the shear stress and increase the work hardening induced dynamic recovery rate, while the high γ_{SFE} of {011} and {001} planes will decrease the dynamic recovery rate. Glide planes of low γ_{SFE} will have the low shear stress which will certainly reduce the gliding velocity of exponential term of dislocations during recovery. T_f is found to be inversely proportional to γ_{SFE} at a constant normal stress. Eqn. 24 has been found to have other constituents, the distance of jog retreat, $f = \lambda b$, which is plane specific and an estimate of kink length lJ = ηb, may be manipulated, using λ constant and η constant. Since dislocations are believed to be mutually recovered by the meeting dislocations of opposite signs and the burger vector is assumed to be a constant for the present context, f is liable to be derived precisely from the planar dislocations spacings, $S_D = \frac{1}{\sqrt{0.5\rho_{hkl}}}$ especially for the crystallographic planes {111}, {110}, and {100}, relying on the science of jog retreat for dynamic recovery.

Dynamic Recovery during Warm Working

Warm working of aluminium alloys is found to stabilize cube and near cube orientations. Stability of certain crystallographic orientations is liable to be addressed by elevated temperature slip activity and crystallographic orientation dependent recovery. Non-compact slip activity at an elevated temperature by cross slip from {111} to {011} and {001} crystallographic planes has been used in simulations but never validated from experiments and the stability of cube and near cube orientations has been found to be higher in classical incompatible Taylor simulator where the compatibility strains are not relaxed. Since, cross slip to {011} and {001} from {111} crystallographic planes requires planar shear strains to be relaxed for mitigating the compatibility in crystal plasticity, the present theory of planar slip on {111}, {011}, and {001} is firmly found, by the existing dislocations on those planes, if permitted by $\gamma_{SFE-hkl}$ [12]. For thermal glide, [7] an advanced theory of dynamic recovery kinetics by nodal jog advancements to facilitate non-conservative cautious to conservative movements of dislocations is inevitable to address the stability of cube and near cube orientations during warm working.

SPD and Dynamic Recovery in Nano Bulk

Control of grain size in alloys is liable to offer an eminent strength, ductility, toughness, superior fatigue resistance, and an excellent shape forming properties [4]. Effect of grain size on properties is still an advanced topic for research [13–15]. Length scale over which dislocation activity occurs in low stacking fault energy FCC alloys, is thin and therefore, very large dislocation pile up by cross slip is formidable [16, 17], may be an extended debated contrary which does not justify the specialty in estimating an extent of long-range strain hardening. Grain boundaries are liable to emit dislocations which glide and get recovered to other grain boundaries [18, 19]. Hence, grain boundaries have been assumed to be an origin and sink of dislocations. Dynamic recovery scenario of dislocations, generally proposed in reports [20, 21], basically conceptualizes as bowing of dislocations from one grain boundary to crystal interior between nodal points and continuous expansion of dislocations prior meeting and get recovered to another grain boundary, may be derivatives of wrong concepts.

Shear stress increases with stacking fault energy, Eqn. 20. Normal stress is an estimated measure for dislocation density. At an exerted constant normal stress, low stacking fault energy glide plane will have high Taylor factor due to less shear stress, Eqn. 19.

Envisaged dynamic recovery analyses are established on an advanced mechanism by rapid nodal jog advancements for non-conservative cautious to conservative movements of dislocations, inevitably required to define an estimate for kink length, lJ and dislocation spacings S_D, Figure 6(a).

Dislocation spacings S_D

$$S_D = \frac{1}{\rho^{\frac{1}{2}}} \tag{41}$$

Energy balance to estimate $l_J$from resolved line tension T_l and stacking fault energy, γ_{SFE}

$$l_J \quad T_l \sin\theta + S_D T_l \cos\theta = \gamma_{SFE} \tag{42}$$

From Eqn. 42,

$$l_J = \frac{\gamma_{SFE} - S_D T_l \cos\theta}{T_l \sin\theta} = \frac{\gamma_{SFE} - \frac{T_l \cos\theta}{\rho^{\frac{1}{2}}}}{T_l \sin\theta} = \frac{(\gamma_{SFE} - \alpha G b \cot\theta)R}{\gamma_{SFE}} = \frac{R}{\mu(\tau)} \tag{43}$$

From Eqns. 17 and 43 for unit jogs $R = b$and $\mu(\tau) = \frac{\gamma_{SFE}}{\gamma_{SFE} - \alpha G b \cot\theta}$ (44)

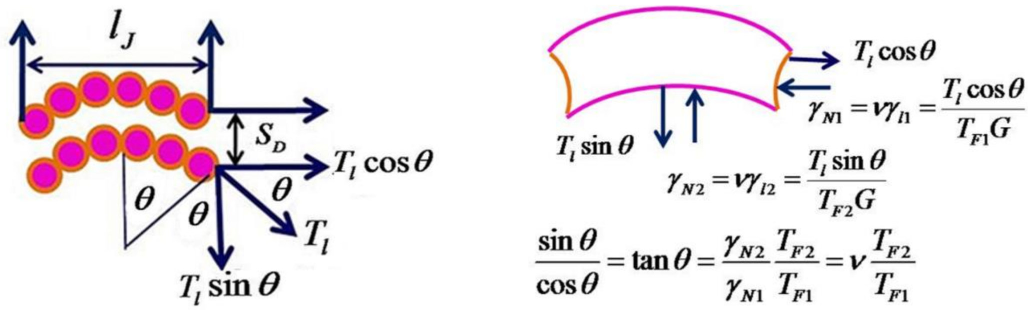

(a) (b)

Figure 6. (a) Stress gradient of stacking fault, an estimate of kink length l_J, dislocation spacings, S_D, angle θ, dislocation spacing is governed by resolved horizontal stress gradient $t_l \cos\theta$ and l_J is governed by resolved vertical stress gradient $t_l \sin\theta$, (b) Ratio to contract an atomic stacking fault, ν, is estimated from resolved stress gradient. γ_{N2} and γ_{N1} are corresponding atomic shear strains for two mutually perpendicular directions in an atomic stacking fault.

Dislocation line tension may be represented by either normal stresses or shear stresses when radius R of dislocation is equal to burger vector of dislocations. Unit jogs are known to have jog length equal to b. Jog density is classically defined by dislocation density. Hence, an extended jog or kink is envisaged to be constituted by many unit jogs of $R = b$, constricted by elastic energy of stacking fault.

For unit jogs, Taylor factor T_{F1} from one atomic displacement, Figure 6 (b), where $R = b$

$$T_{F1} = \frac{\alpha G b^2 \rho^{\frac{1}{2}}}{\gamma_{SFE}} = \frac{\alpha G b^2}{\gamma_{SFE} R} \tag{45}$$

If stress dependent radius of dislocations

$$R = \frac{\mu(\tau) G b^2}{\gamma_{SFE}} \tag{46}$$

From energetic unit jogs, $\sigma = \tau$, therefore from Eqn. 10

$$T_{F1} = 1$$

From Eqns. 16 and 46

$$R = \frac{\alpha G b^2}{\gamma_{SFE}} = \frac{\mu(\tau) G b^2}{\gamma_{SFE}} \tag{47}$$

Therefore,

$$\alpha = \mu(\tau) \tag{48}$$

From Figure 6(b) and Eqn. 43

$$l_J T_l \sin\theta = \gamma_{SFE} - \frac{T_l \cos\theta}{\rho^{\frac{1}{2}}} \tag{49}$$

Dislocation density is derived for an atomic stacking fault for an estimate kink length l_J.

$$\rho^{\frac{1}{2}} = \left(\frac{1}{\frac{\gamma_{SFE}}{T_l \cos\theta} - l_J \tan\theta}\right) = \left(\frac{1}{\frac{R}{\cos\theta} - \frac{R\tan\theta}{\mu(\tau)}}\right) = \frac{1}{R}\left(\frac{\alpha\cos\theta}{\alpha - \cos\theta\tan\theta}\right) \tag{50}$$

$$T_{F2} = \frac{\alpha G b^2 \rho^{\frac{1}{2}}}{\gamma_{SFE}} = \frac{\alpha G b^2}{\gamma_{SFE} R}\left(\frac{\alpha\cos\theta}{\alpha - \cos\theta\tan\theta}\right) \tag{51}$$

where

$$\theta = 2\tan^{-1}\left(\frac{l_J}{2R}\right) \tag{52}$$

Taylor factor emerged to be 1 unit when the normal stresses become shear stresses for unit jogs of radius $R = b$. $\mu(\tau)$ is an extensive co-efficient depending on shear stress τ. Constricted force from lattice on an atomic stacking fault, the radius of an atomic stacking fault is confined to $R = b$ and for that normal trend, an extensive co-efficient $\mu(\tau)$ used to beα. The co-efficient $\mu(\tau)$ is extensively manifested for dislocation line movements and extended in emergence in bulk. Energetics of an atomic stacking fault or an extended stacking fault from perfect lattice is an eminent concern for advanced elevated temperature use of many alloys.

Continuous expansion of bowing out jogs is energetically feasible but liable to be manifested over length regiment rather being mutated on curvature. Therefore, the counteract against retreat of entire kink is an intrinsic dynamic recovery mechanism when pinning jogs energetically advances, as it is to be visualized in reality in broader sense. For nano bulk with an extremely small grain size, the grain boundaries may not act as sinks and become virtually free from ledges [16]. Therefore, an extended dynamic recovery is probable in the nano bulk in grain interior during the movement of kinks. Since work hardening and dynamic recovery defined in SPD is usually conducive for S_D, dislocation spacings and l_J, an extended jog, the range of stress gradient is liable to be infinitesimally limited in reference to nano grain size. Nano bulk forming by SPD [22, 23] usually employs very high stress and increase the working temperature. An extremely faster movement of kinks during SPD is liable to be beyond control by diffusive flux of atoms and therefore, the rate controlling dynamic recovery mechanism inevitably be the thermal glide [7].

CONCLUSIONS

i Industrial new metal working processes require an advanced dislocation density predictive robust simulator to fabricate nano bainite by ausforming and FCC nano bulk by SPD. Proposed recovery simulator is defined to address multi-scale simulation by mean dislocation and orientation dependent dislocation dynamics.

ii T_f is expressed as plane specific γ_{SFE}. γ_{SFE} is found to be inversely proportional to T_f at a constant normal stress. Dynamic recovery rate is found to increase with the decrease in γ_{SFE}. {111} crystallographic planes with less γ_{SFE} will have higher dynamic recovery rate than {110} and {100} crystallographic planes with high γ_{SFE}. Predicted static recovery kinetics by climb of constricted jogs increases with γ_{SFE}, during normalizing though the extent of static recovery during normalizing is never comparative, commensurating rapid dynamic recovery kinetics.

iii Crystallographic dynamic recovery rate has been qualitatively validated from frequency of low angle boundaries, formed in retained austenite, in reference to T_f of an ausformed bainitic steel. Crystallographic orientations with comparatively higher T_f are found to restore the trend of dynamic recovery even after normalizing.

Acknowledgements

Author acknowledges Mr. Ravindra R Malewar, Scientist 'E' and Project Director, Dr. K. Siva Kumar, former Scientist 'G' of ADDD group, for providing ausformed bainitic steel, designed and developed in the project work, High Hardness Bainitic Steel, S&T/15-6/DMRL/DIR3, and Director of DMRL for his continuous encouragement.

Conflicts of Interest

Author declares that he does not have any personal, financial, and other conflicts of interest which have the importance for compromise or bias objectivity of professional judgment.

REFERENCES

1. Humphreys FJ, Hatherly M. Recrystallization and related annealing phenomena. Elsevier: Oxford; 2004.
2. Kubin L, Hoc T, Devincre B. Dynamic recovery and its orientation dependence in face-centered cubic crystals. Acta Mater. 2009; 57(8): 2567–2575.
3. Bacroix B, Brenner R. A phenomenological anisotropic description for dislocation storage and recovery processes in fcc crystals. Comp Mater. Sci. 2012; 54: 97–100.
4. Dieter G. Mechanical metallurgy. SI Metric Ed. London: McGraw-Hill; 1988.
5. M Crumbach M, G Gottstein G. Analysis of the activity of {110}〈110〉 slip in AA3103 by inverse modelling. Mater. Sci. Engg. A. 2004; 387: 282–287.
6. He J, Zhao A, Zhi C, Fan H. Acceleration of nanobainite transformation by multi-step ausforming process, Scripta Mater. 2015; 107: 71–74.
7. Hirth JP, Lothe J. Theory of dislocations. 2nd Ed. John Wiley & Sons: New York; 1982.
8. Hull D, Bacon DJ. Introduction to dislocations. 5th Ed. Elsevier: London; 2011.
9. Radhakrishnan B, Sarma GB. Coupled simulations of texture evolution during deformation and recrystallization of fcc and bcc metals. Mater. Sci. Engg. A. 2008; 494(1–2): 73–79.
10. Umezawa A, Inagaki H. Development of cube recrystallization textures in high-purity Al. International Journal of Materials Research. 2006; 97(1): 49–58.
11. Baudin T, Julliard F, Paillard P, et al. Simulation of primary recrystallization from tem orientation data. Scr. Mater. 2000; 43: 63–68.
12. Vitek V. Stacking faults on {111} and {110} planes in aluminium. Scr. Metall. 1975; 9: 611–615.
13. Koch CC. Ductility in nanostructured and ultra fine grained materials: Recent evidence for optimism. J. Metastable Nanocryst. Mater. 2003; 18: 9–20.
14. Chung CS, Kim JK, Kim HK, et al. Improvement of high-cycle fatigue life in a 6061 Al alloy produced by equal channel angular pressing. Mater. Sci. Engg. A. 2002; 337: 39–44.
15. Tanimoto H, Sakai S, Mizubayashi H. Mechanical property of high density nanocrystalline gold prepared by gas deposition method. Nanostruct. Mater. 1999; 12: 751–756.
16. Meyers MA, Mishra A, Benson DJ. Mechanical properties of nanocrystalline materials. Prog. Mater. Sci. 2006; 51: 427–556.
17. Kumar KS, Swygenhoven HV, Suresh S. Mechanical behavior of nanocrystalline metals and alloys. Acta Mater. 2003; 51: 5743–5774.
18. Swygenhoven HV, Caro A. Plastic behavior of nanophase Ni: A molecular dynamics computer simulation. Appl. Phys. Lett. 1997; 71: 1652–1654.
19. Swygenhoven HV, Derlet PM. Grain-boundary sliding in nanocrystalline fcc metals. Phys. Rev. B. 2001; 64(22): 1–9.
20. Asaro RJ, Krysl P, Kad B. Deformation mechanism transitions in nanoscale fcc metals Phil. Mag. 2003; 83(12): 733–743.
21. Liao XZ, Srinivasan SG, Zhao YH, et al. Formation mechanism of wide stacking faults in nanocrystalline Al. Appl. Phys. Lett. 2004; 84: 3564–3566.
22. Iwahashi Y, Wang JT, Horita Z, et al. Principle of equal-channel angular pressing for the processing of ultra-fine grained materials. Scr. Mater. 1996; 35: 143–146.
23. Valiev RZ, Alexandrov IV. Nanostructured materials from severe plastic deformation. Nanostruct. Mater. 1999; 12: 35–40.

